Hindawi
Complexity
Volume 2022, Article ID 8771583, 19 pages
https://doi.org/10.1155/2022/8771583

Research Article

Abundant Bounded and Unbounded Solitary, Periodic, Rogue-Type Wave Solutions and Analysis of Parametric Effect on the Solutions to Nonlinear Klein–Gordon Model

Mohammad Mobarak Hossain,[1,2] Alrazi Abdeljabbar,[3] Harun-Or Roshid,[1] Md. Mamunur Roshid,[4,5] and Abu Naim Sheikh[2]

[1]*Department of Mathematics, Hamdard University Bangladesh, Bangladesh*
[2]*Department of Mathematics, Dhaka University of Engineering & Technology, Gazipur, Bangladesh*
[3]*Department of Mathematics, Khalifa University, Abu Dhabi, UAE*
[4]*Department of Mathematics, Pabna University of Science and Technology, Pabna-6600, Bangladesh*
[5]*Sunamgonj Science and Technology University, Bangladesh*

Correspondence should be addressed to Md. Mamunur Roshid; harunorroshidmd@gmail.com

Received 21 June 2022; Accepted 23 August 2022; Published 15 October 2022

Academic Editor: Eric Campos

This paper exploits the modified simple equation and dynamical system schemes to integrate the Klein–Gordon (KG) model amid quadratic nonlinearity arising in nonlinear optics, quantum theories, and solid state physics. By implementing the modified simple equation (MSE) technique, we develop some disguise adaptation of analytical solutions in terms of hyperbolic, exponential, and trigonometric functions with some special parameters. We apply the dynamical system to bifurcate the model and draw distinct phase portraits on unlike parametric constraints. Following each orbit of all phase portraits, we originate bounded and unbounded solitary, periodic, and periodic rogue-type wave solutions of the KG model. These two schemes extract widespread classes of solitary, periodic, and periodic rogue-type wave solutions for the KG model jointly due to restrictions on parameters. We also analyze the effect of parameters on the obtained wave solutions and discuss why and when it changes its nature. We illustrate some dynamical features of the acquired solutions via the 3D, 2D, and contour graphics.

1. Introduction

Complex phenomena customarily turned into nonlinear differential equations (NLDEs) by a youngest researcher. Consequently, the study of NLDEs has sustained to attract much effort in the last few years. Many scientific experimental models are employed in nonlinear differential form from the phenomena of nonlinear fiber optics, high-amplitude waves, fluids, plasma, solid state particle motions, etc. Surveying literature, we realized ideas that many scientists worked to disclose innovative, efficient techniques for explaining internal behaviors of NLDEs with constant coefficients that are significant to elucidate different intricate problems such as a discrete algebraic framework [1], IRM-CG method [2], transformed rational function scheme [3], fractional residual method [4], new multistage technique [5], new analytical technique [6], extended tanh approach [7], Hirota-bilinear approach [8–10], multi exp-expansion method [11, 12], Jacobi elliptic expansion method [13, 14], Lie approach [15], Lie symmetry analysis techniques [16], generalized Kudryashov scheme [17, 18], generalized exponential rational function scheme [19], MSE method [20–22], and many more. Such or similar schemes are also used to solve the model with variable coefficients to visualize various new nonlinear dynamics [23–25]. Recently, the nature of rogue waves and diverse dynamical interaction solutions has been studied in numerous fields. There are many researchers who have investigated rogue waves in different fields of mathematical physics and engineering branches [26–32]. Hossain explicated some natures of the solitary and rogue waves with interacting observable facts [26], Ali investigated rogue wave solution from coupled Schrödinger equations [27], and Ohta found general rogue ripple to the discrete nonlinear Schrödinger model [28]. Zhang et al. found rogue wave envelops of $(3+1)$-D Jimbo–Miwa model [29], while Lu et al. established manifold rogue wave envelops for the cKP model [30]. Rogue wave solutions are investigated in the coupled nonlinear Schrödinger models by Degasperis [31], while Ankiewicz found rogue signal elucidations of integrable nonlinear Schrödinger hierarchy [32]. Due to the sensitive effect of a rogue wave, scholars are being highly interested in deriving rogue and such type of colliding wave solutions in the recent exploration [33–36]. Moreover, dynamical researchers have investigated new rogon waves [37], optical M-shaped solitons with interaction with shock waves [38], orbital stability of solitary waves [39], and the nonexistence of global solutions of the time-fractional model [40] newly.

In this survey, we shed light on the quadratic nonlinear dynamics structure, namely, KG, a succeeding structure, which frequently arises in optics, quantum, and solid state physics:

$$u_{tt} - \alpha^2 u_{xx} + \beta u - \gamma u^2 = 0. \tag{1}$$

To analyze the dynamics behavior of solitons in quantum meadow theories, solid state, and nonlinear optical physics, this model is mostly investigated [41–44]. In the last centuries, different dominant and influential schemes have been suggested to execute solutions of the KG equation, such as the Adomian decomposition method [41], auxiliary equation method [42], method of normal forms of Shatah [43], exp-function method [44], and many more. All of the above techniques took the help of an auxiliary equation. But, we need to investigate the internal characteristics of the nonlinear model without the use of other helping equations. Among the above integral techniques, the MSE is better as it never takes any help from the auxiliary equation and can easily solve any nonlinear model with fewer efforts by direct integrations. Besides this, the dynamical system approach is also a directed integral technique that constructs exact solutions according to each energy orbit of its phase portrait. To the best of our knowledge, this considered model was not investigated by such direct integral schemes still now.

Due to this fact, we aim to implement modified simple equation [20–22] and dynamical system schemes [45] on the KG equation to search different types of bounded and unbounded solitary, bright and dark bell envelop, periodic wave, and periodic rouge type wave's solutions of this model with the adequate condition on the exit's parameters.

The rest of the article is organized as follows: in Section 2, we demonstrated analytic solutions of the KG model amid quadratic nonlinearity using the modified simple equation method. Reduction in the dynamical system, bifurcation analysis, and derivation of solutions according to the dynamical scheme is uttered in Section 3. Then, in Section 4, all the deliberated results of the two schemes are illustrated with numerical graphics and explained briefly. In Section 5, we incorporated comparisons and a few remarks with other solutions. The main points of this study are to obtain rogue waves, lump solution, and solitary waves according to energy orbits which are discussed in the last conclusion section.

2. Solutions of KG Model via MSE

In this division, the acquired solutions are an abundant form of traveling wave solutions to the KG model by means of the MSE method [20–22], which might be caring to investigate the different nonlinear representations of turbulence, the wave motions, and a lot of fields such as nonlinear optic, solid state, and plasma physics.

Let us undertake the KG equation with quadratic nonlinearity in the succeeding system [41]. Utilizing the wave transformation relation$\xi = kx - \omega t$and $u(x,t) = U(\xi)$ into Equation (1)which convert the ordinary differential form $u_{tt} = \omega^2 U''$ and $u_{xx} = k^2 U''$. Then using the facts in (1), it reduces as follows:

$$\begin{gathered}\left(\omega^2 - \alpha^2 k^2\right)U'' + \beta U - \gamma U^2 = 0,\\ \text{where}\, U'' = \frac{\mathrm{d}^2 U}{\mathrm{d}\xi^2}.\end{gathered} \tag{2}$$

Now, we allow the MSE method [20–22] to set the solution of (2) as $u(\xi) = \sum_{k=0}^{k=l} a_k (\phi\prime(\xi)/\phi(\xi))^k$, where $a_k\,(k = 0, 1, 2, \ldots, l)$ are free parameters and $a_l \neq 0$ with $l \in \mathfrak{R}^+$ are urbanized from the balancing between the highest order and nonlinear terms eminences in (2).

Here, the power of the series is $l = 2$ obtained from the equilibrium between U'' and U^2. Then, the solution of (2) is studied as

$$U(\xi) = a_0 + a_1\left(\frac{\phi'(\xi)}{\phi(\xi)}\right) + a_2\left(\frac{\phi'(\xi)}{\phi(\xi)}\right)^2. \tag{3}$$

At this instant, including $u(\xi)$ and its derivative form in (2) and considering the coefficient of $\phi(\xi)^{-k}$ $(k = 0, 1, 2 \ldots\ldots)$ equal to zero, it leads to the structure of the algebraic system:

$$\begin{aligned}
&\phi^0(\xi)\colon \beta a_0 - \gamma a_0^2 = 0,\\
&\phi^{-1}(\xi)\colon \left(\omega^2 a_1 - \alpha^2 k^2 a_1\right)\phi''' + \left(\beta a_1 - 2a_1 a_0\right)\phi' = 0,\\
&\phi^{-2}(\xi)\colon \left(\left(-3\omega^2 a_1 S + 3\alpha^2 k^2 a_1\right)\phi'\right.\\
&\qquad + \left(2\omega^2 a_2 - 3\alpha^2 k^2 a_2\right)\phi''\prime\big)\phi'''\\
&\qquad + \left(\left(2\omega^2 a_2 - \gamma a_1 - 2\alpha^2 k^2 a_2\right)\phi'''\right.\\
&\qquad \left(-2\gamma a_1 a_0 + \beta a_1\right)\phi'\big)\phi' = 0,\\
&\phi^{-3}(\xi)\colon \left(-2\gamma a_1 a_2 + 2\omega^2 a_1 - 2\alpha^2 k^2 a_1\right)\phi'\\
&\qquad + \left(10\alpha^2 k^2 a_2 - 10\omega^2 a_2\right)\phi'' = 0,\\
&\phi^{-4}(\xi)\colon \left(6\omega^2 a_2 - 6\alpha^2 k^2 a_2 - \gamma a_2^2\right)\phi^{iv} = 0.
\end{aligned} \tag{4}$$

The coefficient of $\phi^0(\xi)$ and $\phi^{-4}(\xi)$ brings out two set solutions,

Set-01: $a_0 = 0, a_2 = 6\omega^2 - 6\alpha^2k^2/\gamma$.

Set-02: $a_0 = \beta/\gamma, a_2 = 6\omega^2 - 6\alpha^2k^2/\gamma$

Now, we insert the value of a_0 and a_2 from set-01 in the remaining equations and resolve them with the assistance of Maple which gives

$$\begin{aligned}
&\phi(\xi) = c_1 + c_2 \exp\left(\frac{a_1\gamma\xi}{-6\omega^2 + 6\alpha^2k^2}\right), \mathfrak{A}\\
&\omega = \pm\frac{\sqrt{-\beta\left(-36\beta\alpha^2k^2 + a_1^2\gamma^2\right)}}{6\beta},\\
&a_1 = a_1, k = k,
\end{aligned} \tag{5}$$

$$\begin{aligned}
&\phi(\xi) = c_1 + c_2 \exp\left(\frac{a_1\gamma\xi}{-6\omega^2 + 6\alpha^2k^2}\right),\\
&a_1 = 6\sqrt{\frac{\alpha^2k^2 - \omega^2}{\gamma^2}},\\
&\omega = \omega, k = k.
\end{aligned} \tag{6}$$

Case-01: while equation (4) is treated and making use of the values in equation (3), acquiesce

$$U(\xi) = \frac{6\beta c_1c_2e^\theta}{\gamma\left(c_1 + c_2e^\theta\right)^2}, \tag{7}$$

where $\theta = -a_1\gamma\xi/6\omega^2 - 6\alpha^2k^2$, $\xi = kx- \sqrt{-\beta(-36\beta\alpha^2k^2 + a_1^2\gamma^2)}/6\beta t$, and a_1, k, β, α, and γ are arbitrary constant.

Whenever $c_1 \neq c_2$, and the condition $\beta < 0$ and $a_1^2\gamma^2 < 36\beta\alpha^2k^2$ or $\beta > 0$ and $a_1^2\gamma^2 > 36\beta\alpha^2k^2$, then solution (7) can be expressed in trigonometric function solution in the following form:

$$U(\xi) = \frac{6\beta c_1c_2}{\gamma\left(2c_1c_2 + \cos\theta\left(c_1^2 + c_2^2\right) - i\sin\theta\left(c_1^2 - c_2^2\right)\right)}. \tag{8}$$

Inserting $c_1 = \pm c_2$ in (8), it develops in the succeeding form:

$$U(\xi) = \pm\frac{3\beta}{2\gamma}\sec^2\left(\frac{\theta}{2}\right). \tag{9}$$

Setting $c_1 = \pm ic_2$ in (8), then the solution becomes

$$u(\xi) = \frac{3\beta}{\gamma(i \pm \sin\theta)}. \tag{10}$$

Whenever $c_1 \neq c_2$ and reflects on the condition $\beta < 0$ and $a_1^2\gamma^2 > 36\beta\alpha^2k^2$, the solution (7) gathers in hyperbolic form as

$$U(\xi) = \frac{6\beta c_1c_2}{\gamma\left(2c_1c_2 + \cosh\theta\left(c_1^2 + c_2^2\right) - \sinh\theta\left(c_1^2 - c_2^2\right)\right)}. \tag{11}$$

Inserting $c_1 = \pm c_2$ in (11), then the solution reduces to

$$U(\xi) = \pm\frac{3\beta}{2\gamma}\sec h^2\left(\frac{\theta}{2}\right). \tag{12}$$

Substituting set $c_1 = \pm ic_2$, then (11) is

$$U(\xi) = \pm\frac{3\beta}{\gamma(1\mp i\sinh\theta)}. \tag{13}$$

Case-02: while equation (5) is treated and making use of the values in equation (3), we acquiesce

$$U(\xi) = \frac{6\beta c_1c_2e^\theta}{\gamma\left(c_1 + c_2e^\theta\right)^2}, \tag{14}$$

where $\theta = \gamma^2\xi/\sqrt{\alpha^2k^2 - \omega^2}$, $\xi = kx - \omega t$, and $\gamma, \alpha, k, \omega$ are arbitrary constant.

Making use of $c_1 \neq c_2$ and $\alpha^2k^2 < \omega^2$ in (14), then the solution is expressed in trigonometric function solution in the following form:

$$U(\xi) = \frac{6\beta c_1c_2}{\gamma\left(2c_1c_2 + \cos\theta\left(c_1^2 + c_2^2\right) - i\sin\theta\left(c_1^2 - c_2^2\right)\right)}. \tag{15}$$

Inserting $c_1 = \pm c_2$ in (15), the solution is

$$U(\xi) = \pm\frac{3\beta}{2\gamma}\sec^2\left(\frac{\theta}{2}\right). \tag{16}$$

Employing $c_1 = \pm ic_2$ in (15), then the solution develops as

$$U(\xi) = \frac{3\beta}{\gamma(i \pm \sin\theta)}. \tag{17}$$

Making use of $c_1 \neq c_2$ and $\alpha^2k^2 > \omega^2$ in (14), then the solution is expressed in hyperbolic function solution in the following form:

$$U(\xi) = \frac{6\beta c_1c_2}{\gamma\left(2c_1c_2 + \cosh\theta\left(c_1^2 + c_2^2\right) + \sinh\theta\left(c_1^2 - c_2^2\right)\right)}. \tag{18}$$

Inserting $c_1 = \pm c_2$ in (18), the solution takes the form

$$U(\xi) = \pm\frac{3\beta}{2\gamma}\sec h^2\left(\frac{\theta}{2}\right). \tag{19}$$

Employing $c_1 = \pm ic_2$ in (18), then the solution develops as

$$U(\xi) = \frac{3\beta}{\gamma(i\mp\sinh\theta)}, \tag{20}$$

where $\theta = \sqrt{\beta/\alpha^2k^2 - \omega^2}\xi, \xi = kx - \omega t, \alpha, k, \omega, \beta$, and γ are arbitrary constant.

Set-02: if $a_0 = \beta/\gamma, a_2 = 6\omega^2 - 6\alpha^2k^2/\gamma$.

Inserting the value of a_0 and a_2 from set-02 in the enduring equations and resolving them, then we gather the solution in the following form:

$$\phi(\xi) = c_1 + c_2 \exp(\xi),$$
$$k = \frac{\sqrt{\omega^2 - \beta}}{\alpha}, \tag{21}$$
$$a_1 = \pm \frac{6\beta}{\gamma}.$$

Now, the above values are placed in solution (3).

$$U(\xi) = \frac{\beta}{\gamma} - \frac{6\beta}{\gamma}\left(\frac{c_2 e^{\xi}}{c_1 + c_2 e^{\xi}}\right) + \frac{6\beta}{\gamma}\left(\frac{c_2 e^{\xi}}{c_1 + c_2 e^{\xi}}\right)^2, \tag{22}$$

where $\xi = \sqrt{\omega^2 - \beta}/\alpha x - \omega t$, and $\beta, \omega, \gamma, \alpha$ are arbitrary constants.

Whenever $c_1 \neq c_2$ and the condition $\omega^2 < \beta$, then solution (22) brings out in the trigonometric form

$$U(\xi) = \frac{\beta}{\gamma} - \frac{6\beta c_1 c_2}{\gamma\left(2c_1c_2 + \cos\xi\left(c_1^2 + c_2^2\right) + i\sin\xi\left(c_1^2 - c_2^2\right)\right)}, \tag{23}$$

where $\xi = \sqrt{-\omega^2 + \beta}/\alpha + i\omega t$ and β, k, γ, α are arbitrary constant.

Inserting $c_1 = \pm c_2$ in (23), then the solution develops as

$$U(\xi) = \frac{\beta}{\gamma} \mp \frac{3\beta}{2\gamma}\sec^2\left(\frac{\xi}{2}\right). \tag{24}$$

Putting $c_1 = \pm i c_2$ in (23), then the solution is

$$U(\xi) = \frac{\beta}{\gamma} \mp \frac{3\beta}{\gamma(i \pm \sin\xi)}. \tag{25}$$

Whenever $c_1 \neq c_2$ and the condition $\beta < \omega^2$, then (22) can be transcribed in hyperbolic form

$$U(\xi) = \frac{\beta}{\gamma} - \frac{6\beta c_1 c_2}{\gamma\left(2c_1c_2 + \cosh\xi\left(c_1^2 + c_2^2\right) + \sinh\xi\left(c_1^2 - c_2^2\right)\right)}. \tag{26}$$

Making use of $c_1 = \pm c_2$ into (26) yields

$$U(\xi) = \frac{\beta}{\gamma} \mp \frac{3\beta}{2\gamma}\sec h^2\left(\frac{\xi}{2}\right). \tag{27}$$

If $c_1 = \pm i c_2$, then solution (26) is

$$U(\xi) = \frac{\beta}{\gamma} \mp \frac{3\beta}{\gamma(1 \pm i\sinh\xi)}. \tag{28}$$

3. Bifurcation Analysis and Solutions for Each Orbit of the Phase Portraits

In this part, we shed light on bifurcating the KG model due to the involve parameters, and various phase portraits are derived depending on dissimilar conditions of the parameters. We also establish diverse soliton, periodic, and superperiodic solutions according to each energy orbit of the phase portrait. Here, we draw this action spiting the work into two subsections as follows.

3.1. Bifurcations and Phase Portraits of the KG Model. Recall (2) that can be rewritten into a system of dynamical form

$$\begin{aligned} U' &= V = F(U,V), \\ V' &= -\frac{\beta}{\omega^2 - \alpha^2k^2}U + \frac{\gamma}{\omega^2 - \alpha^2k^2}U^2 = G(U,V), \end{aligned} \tag{29}$$

which has Hamiltonian energy states as

$$H(U,V) = \frac{V^2}{2} + \frac{\beta}{\omega^2 - \alpha^2k^2}\frac{U^2}{2} - \frac{\gamma}{\omega^2 - \alpha^2k^2}\frac{U^3}{3} = \hbar. \tag{30}$$

Next, we make an effort to perceive phase orbits of (29) with various situations on the parameters $\alpha, \beta, \gamma, k, \omega$. Deriving critical points in an equilibrium situation, we have to consider $U' = 0$ and $V' = 0$, then the prototype (29) will provide two equilibrium points $\sigma(0,0)$ and $\tau(\beta/\gamma, 0)$, if $\beta \neq 0$. Besides this, the dynamical archetype (29) acquiesced only one critical point $\sigma(0,0)$ for $\beta = 0$. The Jacobian of each critical points is as follows (Figure 1(a)).

$$\begin{aligned} J_{\sigma(0,0)} &= \frac{\beta}{\omega^2 - \alpha^2k^2}, \\ J_{\tau(U,0)} &= -\frac{\beta}{\omega^2 - \alpha^2k^2}, \\ \operatorname{Trace}(A(\sigma)) &= 0, \\ \operatorname{Trace}(A(\tau)) &= 0. \end{aligned} \tag{31}$$

According to the bifurcation theorem [45] and our inspection, we acquire the subsequent annotations.

Cluster-1 For both $\beta > 0$, $\omega^2 - \alpha^2k^2 > 0$ and $\beta < 0$, $\omega^2 - \alpha^2k^2 < 0$, we present a nature with the origin $\sigma(0,0)$ which is a stable center point and $\tau(\beta/\gamma, 0)$ is a saddle point, whereas the corresponding bifurcations of phase portraits of the prototype (29) are visualized in Figure 1(a) and 1(b), respectively. Phase portraits (Figure 1(a) and 1(b)) are drawn for $\alpha = 1, \omega = 2, \beta = 4, \gamma = 1, k = 1$ and $\alpha = 1, \omega = 2, \beta = 4, \gamma = -1, k = 1$, respectively. Besides this, $\gamma > 0$ and $\gamma < 0$ just alter the directions of flow.

Cluster-2: for $\beta > 0$, $\omega^2 - \alpha^2k^2 < 0$ and $\beta < 0$, $\omega^2 - \alpha^2k^2 > 0$, we present a nature with the origin $\sigma(0,0)$ which is a saddle point and $\tau(\beta/\gamma, 0)$ is a stable center point, whereas the corresponding bifurcations of phase portraits of the prototype (29) are depicted in Figure 2(b), respectively. Phase portraits (Figures 2(a) and 2(b)) are drawn for $\alpha = 1, \omega = 2, \beta = -4, \gamma = 1, k = 1$ and $\alpha = 1, \omega = 2, \beta = -4, \gamma = -1, k = 1$, respectively. Besides this, $\gamma > 0$ and $\gamma < 0$ just alter the directions of flow.

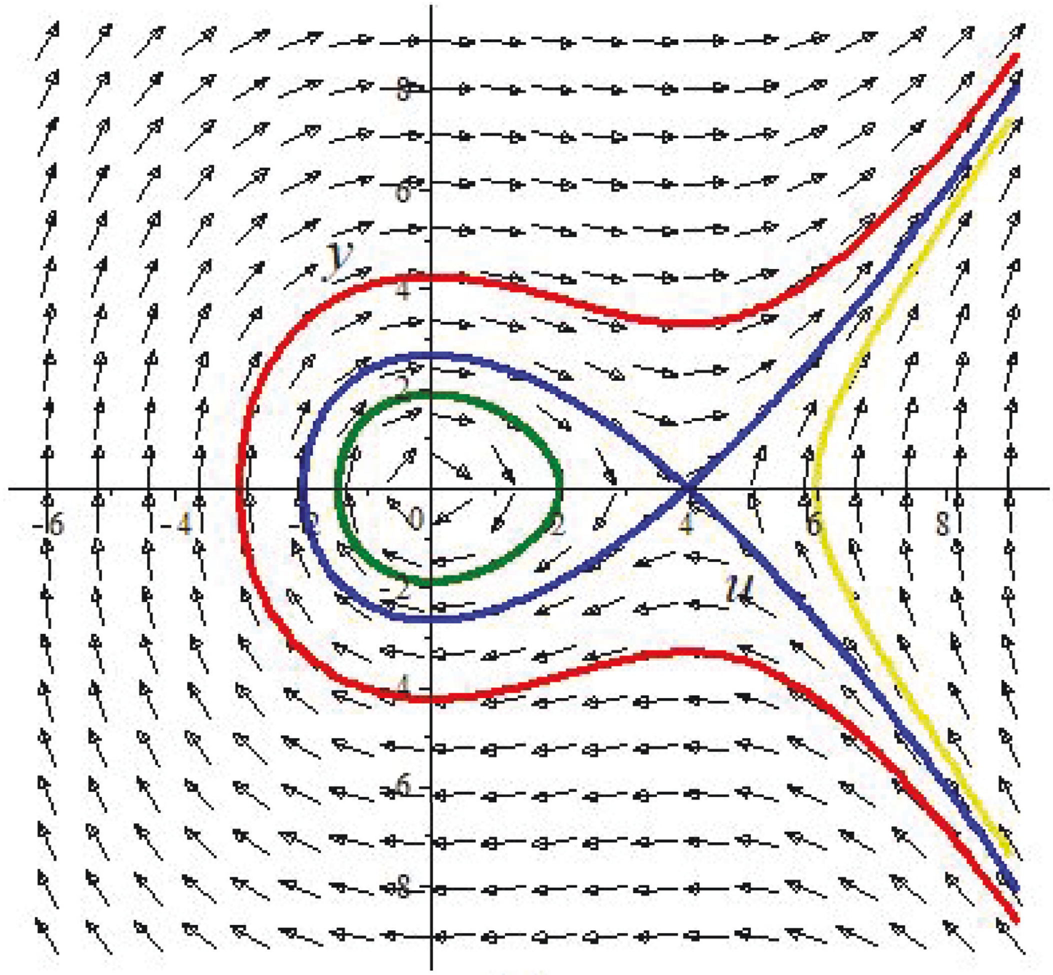

(a)

Figure 1: Continued.

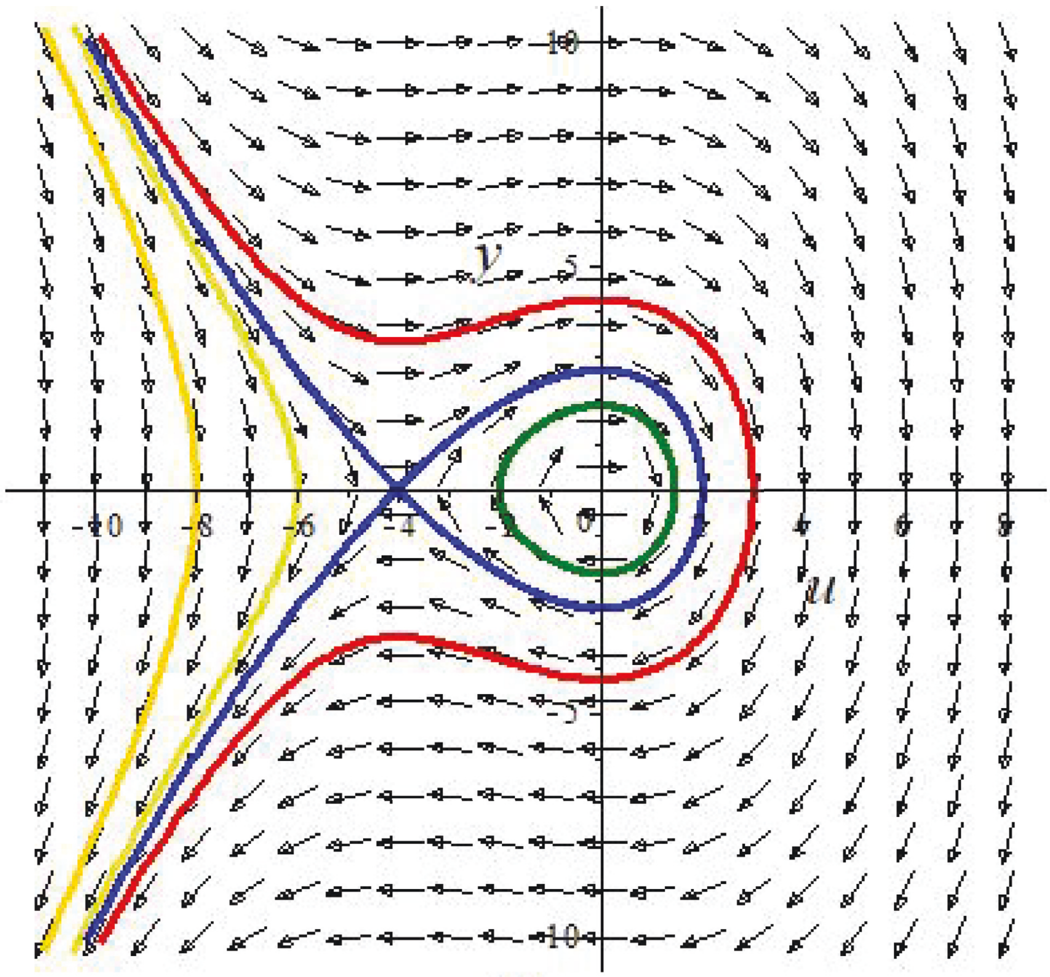

(b)

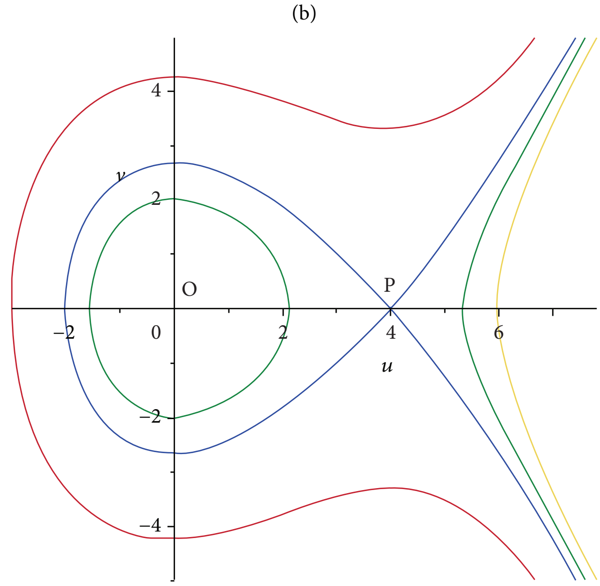

(c)

Figure 1: (a) Phase portrait on $\beta > 0, \omega^2 - \alpha^2 k^2 > 0, \gamma > 0$ or $\beta < 0, \omega^2 - \alpha^2 k^2 < 0, \gamma < 0$. (b) Phase portrait on $\beta > 0, \omega^2 - \alpha^2 k^2 > 0, \gamma < 0$ or $\beta < 0, \omega^2 - \alpha^2 k^2 < 0, \gamma > 0$. (c) Phase portrait from Hamiltonian for $\alpha = 1, \omega = 2, \beta = 4, \gamma = 1, k = 1$.

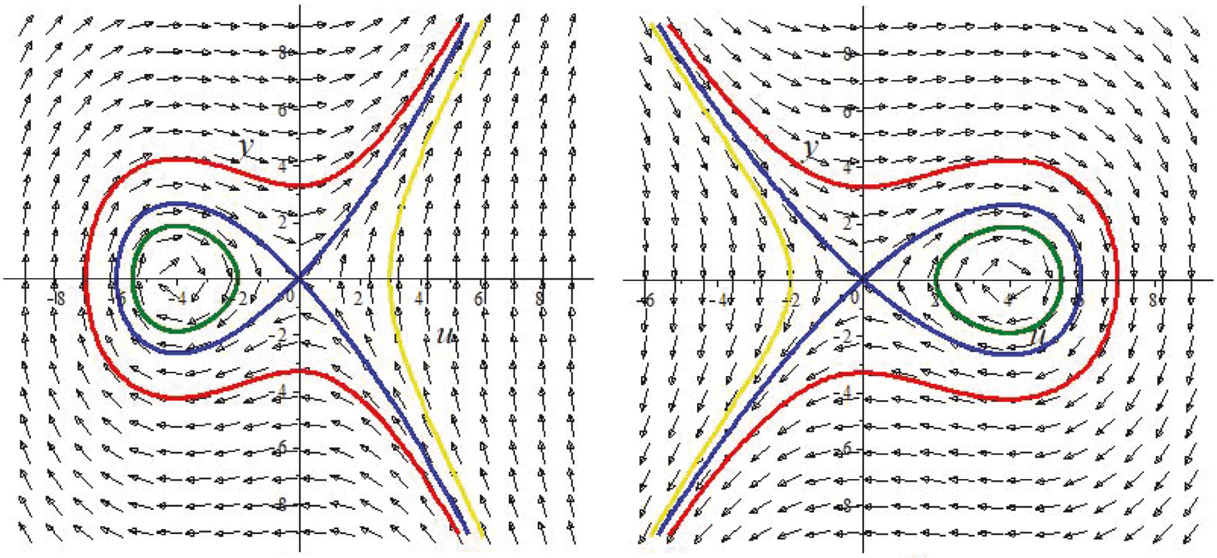

(a) (b)

Figure 2: (a) Phase portrait on $\beta < 0, \omega^2 - \alpha^2k^2 > 0, \gamma > 0$ or $\beta > 0, \omega^2 - \alpha^2k^2 < 0, \gamma < 0$. (b) Phase portrait on $\beta < 0, \omega^2 - \alpha^2k^2 > 0, \gamma < 0$ or $\beta > 0, \omega^2 - \alpha^2k^2 < 0, \gamma > 0$..

Cluster-3: for $\beta = 0$, the nature at origin $N_0(0,0)$ is a cusp point, whereas the corresponding bifurcations of phase portraits of the prototype (29) are depicted, respectively. In this case, both $\gamma > 0$, $\omega^2 - \alpha^2k^2 > 0$ and $\gamma < 0$, $\omega^2 - \alpha^2k^2 < 0$ exhibit the same directions of flow, but an opposite sign that is $\gamma > 0$, $\omega^2 - \alpha^2k^2 < 0$ or $\beta < 0$, $\omega^2 - \alpha^2k^2 > 0$ exhibits altered directions of flow. Phase portraits (Figures 3(a) and 3(b)) are drawn for $\alpha = 1, \omega = 2, \gamma = 1, k = 1$ and $\alpha = 1, \omega = 2, \gamma = -1$, $k = 1$, respectively.

3.2. Precise Solutions for Model (1). Here, we develop a variety of precise parametric representations of wave solutions of the model (1). For facility, we first draw out the energy stages via Hamiltonian of the model, which is identified by equation (29) with separated various regions due to the energy level of the critical points (Figures 2(a), 3(a), and 3(b):

$$\hbar_\sigma = H(0,0) = 0,$$
$$\hbar_\tau = H\left(\frac{\beta}{\gamma}, 0\right) = \frac{\beta^3}{6\gamma^2\left(\omega^2 - \alpha^2k^2\right)}. \tag{32}$$

3.2.1. Solutions for Cluster-1

(i) On the parametric situation $\beta > 0, \omega^2 - \alpha^2k^2 > 0$, $\gamma > 0$ or $\beta < 0, \omega^2 - \alpha^2k^2 < 0, \gamma < 0$, the linked homoclinic orbit (see blue curve in Figure 1(a) at $\tau(\beta/\gamma, 0)$ is illustrated via $H(U,V) = \hbar_\tau$, which suggests a valley type smooth solitary wave solution. The orbit $H(U,V) = \hbar_\tau = \beta^3/6\gamma^2(\omega^2 - \alpha^2k^2)$ in equation (29) yields

$$V = \pm\sqrt{\frac{2\gamma}{3\left(\omega^2 - \alpha^2k^2\right)}}\left(U - \frac{\beta}{\gamma}\right)\sqrt{U + \frac{\beta}{2\gamma}}. \tag{33}$$

We merge the first equation of (29) and (33) with integration; we attain a valley-type smooth solitary wave solution

$$u(x,t) = \left|\frac{\beta}{2\gamma}\right|\left(-1 + 3\tanh^2\left(\sqrt{\frac{\beta}{4\left(\omega^2 - \alpha^2k^2\right)}}|\xi|\right)\right),$$
where $\xi = kx - \omega t$.
$$\tag{34}$$

(iii) On the parametric situation $\beta > 0, \omega^2 - \alpha^2k^2 > 0$, $\gamma < 0$ or $\beta < 0, \omega^2 - \alpha^2k^2 < 0, \gamma > 0$ the linked homoclinic orbit (see blue curve in Figure 1(b) at $\tau(\beta/\gamma, 0)$ is illustrated via $H(U,V) = \hbar_\tau$, which suggests a valley-type smooth solitary wave solution. The orbit $H(U,V) = \hbar_\tau = \beta^3/6\gamma^2(\omega^2 - \alpha^2k^2)$ in equation (29) yields

$$V = \pm\sqrt{\frac{2\gamma}{3\left(\alpha^2k^2 - \omega^2\right)}}\left(U + \frac{\beta}{\gamma}\right)\sqrt{\frac{\beta}{2\gamma} - U}. \tag{35}$$

We merge the first equation of (29) and (35) with integration; we attain a valley-type smooth solitary wave solution

$$u(x,t) = \left|\frac{\beta}{2\gamma}\right|\left(1 - 3\tanh^2\left(\sqrt{\frac{\beta}{4\left(\omega^2 - \alpha^2k^2\right)}}|\xi|\right)\right),$$
where $\xi = kx - \omega t$.
$$\tag{36}$$

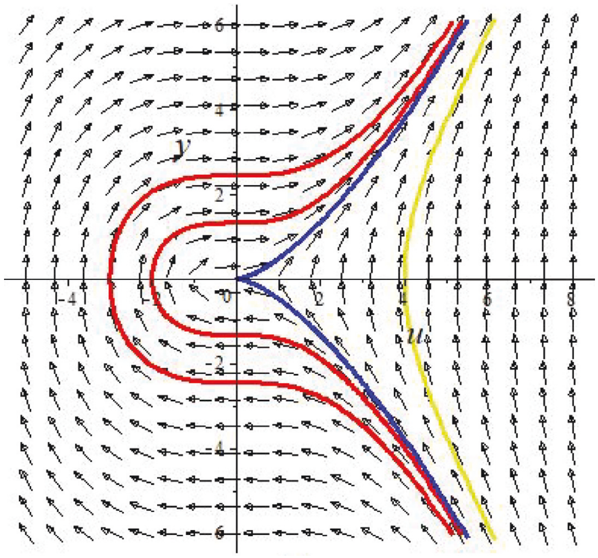

(a)

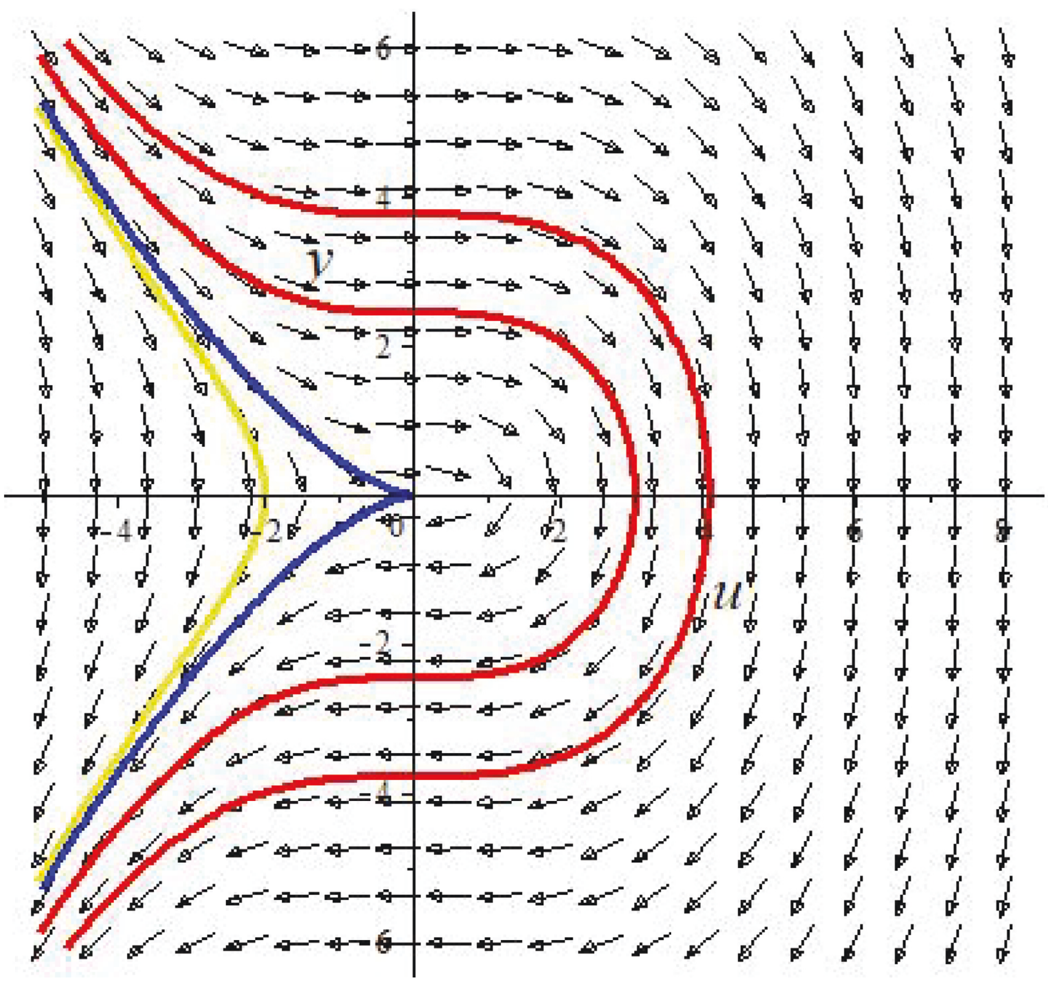

(b)

FIGURE 3: (a) When $\omega^2 - \alpha^2 k^2 > 0, \gamma > 0$ or $\omega^2 - \alpha^2 k^2 < 0, \gamma < 0$. (b) When $\omega^2 - \alpha^2 k^2 > 0, \gamma < 0$ or $\omega^2 - \alpha^2 k^2 < 0, \gamma > 0$.

(iii) On the parametric situation $\beta > 0, \omega^2 - \alpha^2 k^2 > 0, \gamma > 0$ or $\beta < 0, \omega^2 - \alpha^2 k^2 < 0, \gamma < 0$, the model (1) corresponds to a family of periodic orbits that provide periodic wave solutions expressed by $H(U, V) = \hbar_\tau, \hbar \in (0, \hbar_\tau)$ (see the green color orbit in Figure 1(a) or phase portrait in Figure 1(c)). For this situation, equation (29) of the closed domain can be written as follows:

$$V = \pm \sqrt{2\gamma/3(\omega^2-\alpha^2k^2)}\sqrt{(U-\ell_1)(\ell_2-U)(\ell_3-U)},$$

(36), where $(\ell_1,0)$, $(\ell_2,0)$, and $(\ell_3,0)$ are the cutting points by the orbits $H(U,V)=\hbar, \hbar\in(0,\hbar_\tau)$ on the U-axis that preserve the condition $-\beta/2\gamma\le\ell_1<U<\ell_2(\le\beta/\gamma)<\ell_3$. Merging the first equation of (28) and (36), we gain the periodic solution as follows:

$$u(x,t)=\ell_1+(\ell_2-\ell_1)sn^2\left(\sqrt{\frac{\gamma(\ell_3-\ell_1)}{6(\omega^2-\alpha^2k^2)}}|\xi|,\sqrt{\frac{(\ell_1-\ell_2)}{(\ell_1-\ell_3)}}\right). \quad (37)$$

On the parametric situation $\beta<0,\omega^2-\alpha^2k^2>0,\gamma<0$ or $\beta>0,\omega^2-\alpha^2k^2<0,\gamma>0$, similar investigation on Figure 1(b) provide us with three intersecting points $(\ell_4,0)$, $(\ell_5,0)$, and $(\ell_6,0)$ identified by the orbits $H(U,V)=\hbar, \hbar\in(\hbar_\tau,0)$ on the U-axis that preserve the condition $\ell_4<(\beta/\gamma\le)\ell_5<U<\ell_6;\gamma<0$.

We acquire the parametric formulation of the periodic solution as follows:

$$u(x,t)=\ell_4+\frac{(\ell_4-\ell_5)(\ell_6-\ell_4)}{(\ell_6-\ell_5)sn^2\left(\sqrt{\gamma(\ell_4-\ell_6)/6(\omega^2-\alpha^2k^2)}|\xi|,\sqrt{(\ell_6-\ell_5)/(\ell_6-\ell_4)}\right)-(\ell_6-\ell_4)}. \quad (38)$$

3.2.2. Solutions for Cluster-2

(i) On the parametric situation $\beta<0,\omega^2-\alpha^2k^2>0,\gamma>0$ or $\beta>0,\omega^2-\alpha^2k^2<0,\gamma<0$, the model (1) corresponds to a homoclinic orbit (see the blue curve in Figure 2(a)) at the point $\sigma(0,0)$ identified by $H(U,V)=\hbar_\sigma=0$, where the prototype (28) suggests itself as a smooth solitary wave solution of valley type. The assistance of the relation $H(U,V)=\hbar_\sigma=0$ in equation (29) yields

$$V=\pm\sqrt{\frac{2\gamma}{3(\omega^2-\alpha^2k^2)}}U\sqrt{U-\frac{3\beta}{2\gamma}}. \quad (39)$$

Then, merging the first equation of (29) and (39) yields the valley-type smooth solitary wave solution:

$$u(x,t)=\left|\frac{3\beta}{2\gamma}\right|\left(\tanh^2\left(\sqrt{\frac{-\beta}{4(\omega^2-\alpha^2k^2)}}|\xi|\right)-1\right), \quad (40)$$

where $\xi=kx-\omega t$.

(ii) On the parametric situation $\beta>0,\omega^2-\alpha^2k^2<0,\gamma>0$ or $\beta<0,\omega^2-\alpha^2k^2>0,\gamma<0$, the model (1) corresponds to a homoclinic orbit (see the blue curve in Figure 2(b)) at the point $\sigma(0,0)$ identified by $H(U,V)=\hbar_\sigma=0$, where the prototype (28) suggests itself as a smooth solitary wave solution of valley -type. The assistance of the relation $H(U,V)=\hbar_\sigma=0$ in equation (29) yields

$$V=\pm\sqrt{\frac{2\gamma}{3(\alpha^2k^2-\omega^2)}}U\sqrt{\frac{3\beta}{2\gamma}-U}. \quad (41)$$

Then, merging the first equation of (29) and (41) yields the valley-type smooth solitary wave solution:

$$u(x,t)=\left|\frac{3\beta}{2\gamma}\right|\left(1-\tanh^2\left(\sqrt{\frac{-\beta}{4(\omega^2-\alpha^2k^2)}}|\xi|\right)\right), \quad (42)$$

where $\xi=kx-\omega t$.

(iii) On the parametric situation $\beta<0,\omega^2-\alpha^2k^2>0,\gamma>0$ or $\beta>0,\omega^2-\alpha^2k^2<0,\gamma<0$, the prototype (28) has a set of smooth periodic wave solutions identified by $H(U,V)=\hbar$, which can be observed in Figure 2(a)$\hbar\in(\hbar_\tau,0)$, and on situation $\beta>0,\omega^2-\alpha^2k^2<0,\gamma>0$ or $\beta<0,\omega^2-\alpha^2k^2>0,\gamma<0$, Figure 2(b) for $\hbar\in(0,\hbar_\tau)$, respectively. For this aspect, the formulation of the periodic solution is identical to the solutions in equations (37) and (38), respectively.

3.2.3. Solutions for Cluster-3

(i) On the state $\beta=0,\omega^2-\alpha^2k^2>0,\gamma>0$ or $\beta=0,\omega^2-\alpha^2k^2<0,\gamma<0$, there is an unrestricted orbit with the alike Hamiltonian at the origin $\sigma(0,0)$ (Figure 3(a)). This open cusp orbit (blue color) can be précised by

$$V=\pm\sqrt{\frac{2\gamma}{3(\omega^2-\alpha^2k^2)}}U^{3/2}. \quad (43)$$

Then, by facilitation of the first equation of the prototypes (29) and (43), we get hold of the periodic cusp wave solution as follows:

$$u(x,t)=\left|\frac{6(\omega^2-\alpha^2k^2)}{\gamma}\right|\frac{1}{\xi^2}, \quad (44)$$

where $\xi=kx-\omega t$.

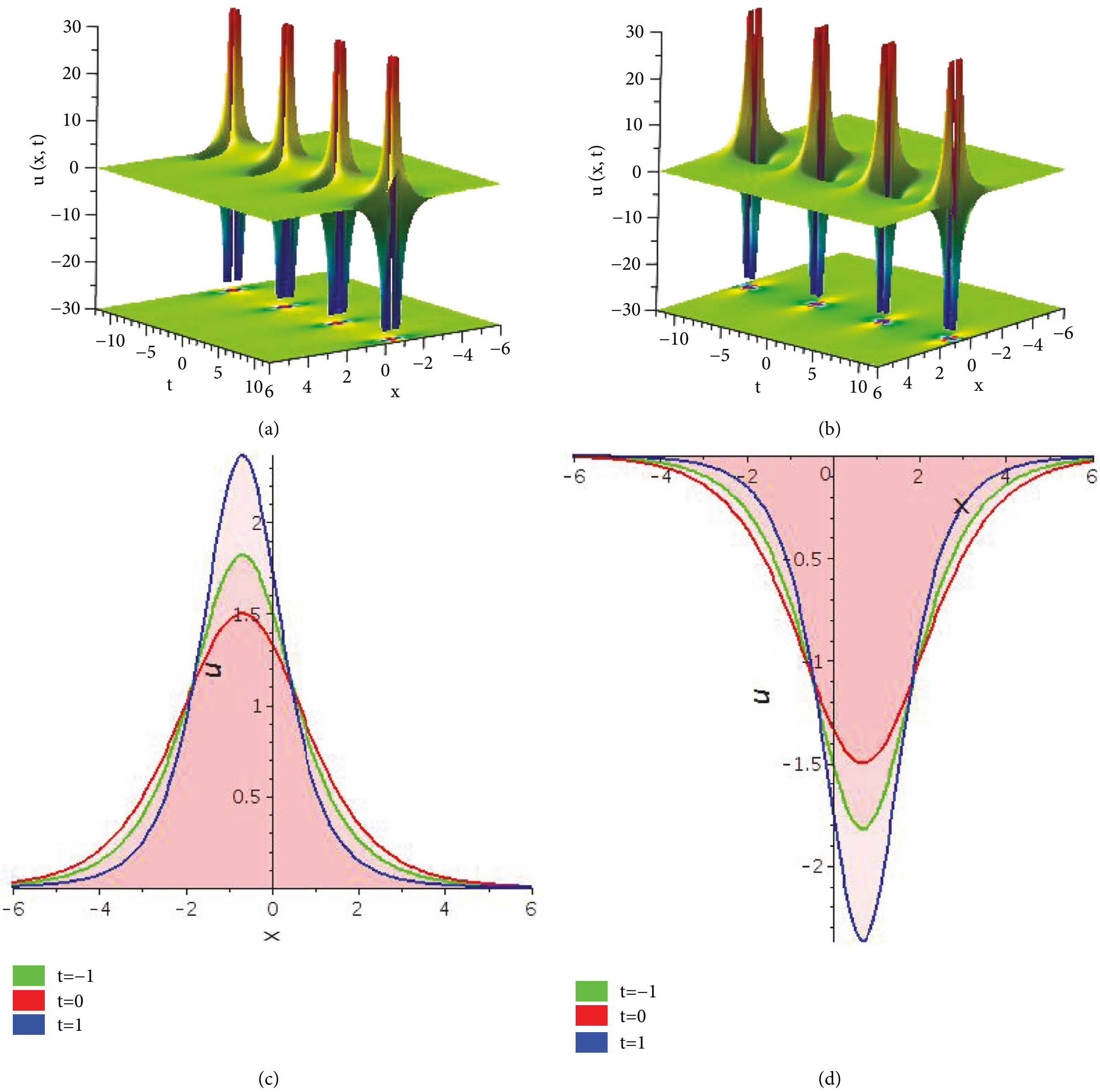

FIGURE 4: This is shape periodic rogue-type lump wave of the real part of the solution (7) through the value of parameters $c_1 = 1, c_2 = 2, k = \alpha = 0.5, a_1 = 3, \gamma = 1, \beta = 1$. The periodicity exists along the t-axis: (i) 3D contour plot; (ii) density plot; (iii) 2D plot.

(ii) On the state $\beta = 0, \omega^2 - \alpha^2k^2 > 0, \gamma < 0$ or $\beta = 0, \omega^2 - \alpha^2k^2 < 0, \gamma > 0$, there is also an unrestricted orbit with the alike Hamiltonian as the origin $\sigma(0,0)$ (Figure 3(b)). Due to this condition, we also catch out the similar periodic cusp wave solution in the form

$$u(x,t) = -\left|\frac{6(\omega^2 - \alpha^2k^2)}{\gamma}\right|\frac{1}{\xi^2}, \tag{45}$$

where $\xi = kx - \omega t$.

4. Results and Discussion

4.1. Solutions via Modified Simple Equation Method. For the assorted values of the appreciate constants, we achieved rogue wave multilump wave, dark and bright bell shape solution, singular and antisingular soliton, and m-type and anti-m-type periodic solutions. Those solutions are obliging to investigate a different nonlinear model of turmoil, the wave motions, and a lot of fields such as nonlinear optic, solid, and plasma state physics. We also set the parametric conditions for which the same solutions behave dissimilarly on the change of their parametric values.

Here are the solutions (7), (8), (9), (13), (14), (15), (22), (23), and (24) which arrived in the form of a trigonometric function, and the solutions (10), (11), (12), (17), (18), (19),

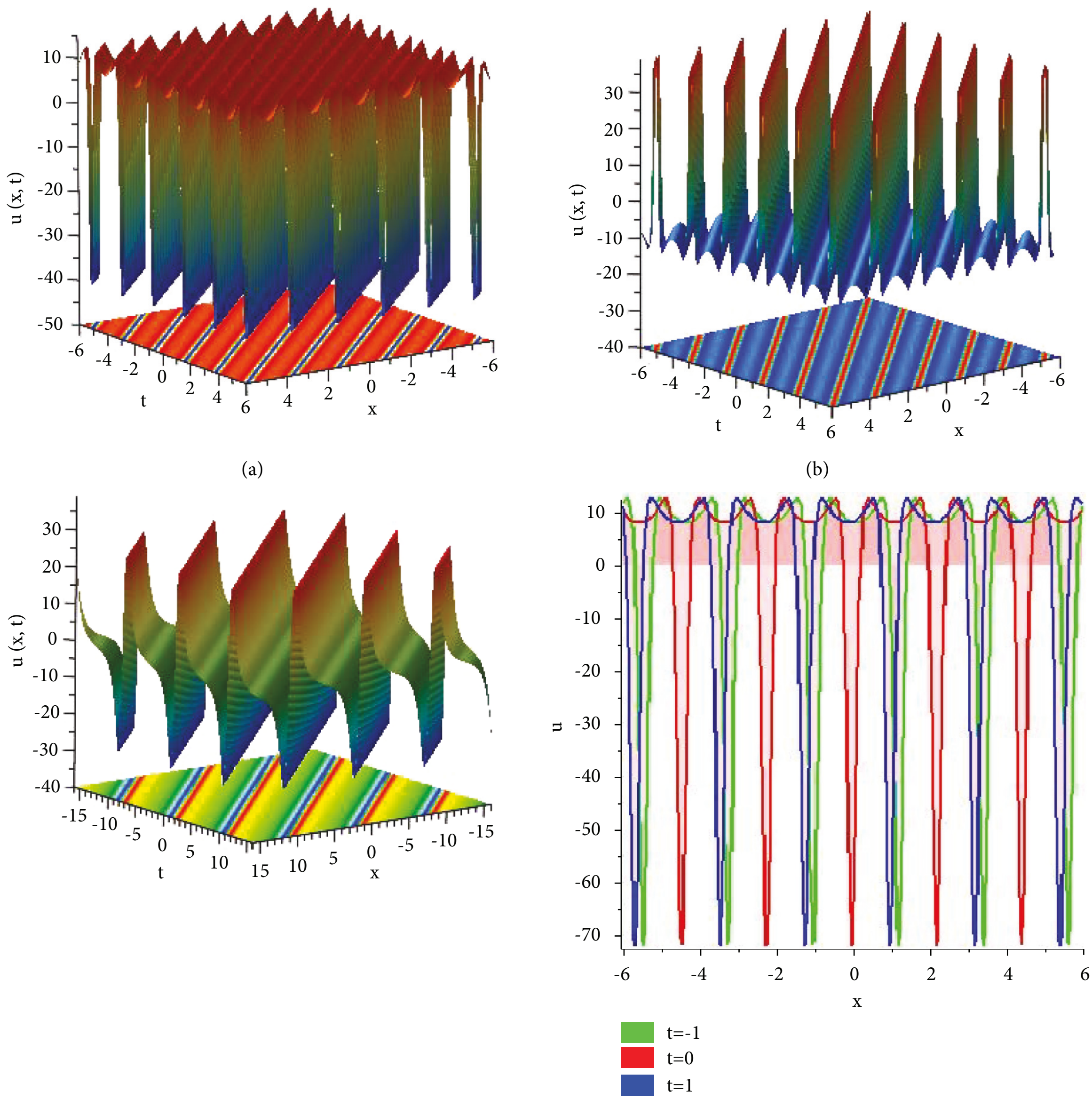

(a) (b) (c) (d)

Figure 5: Continued.

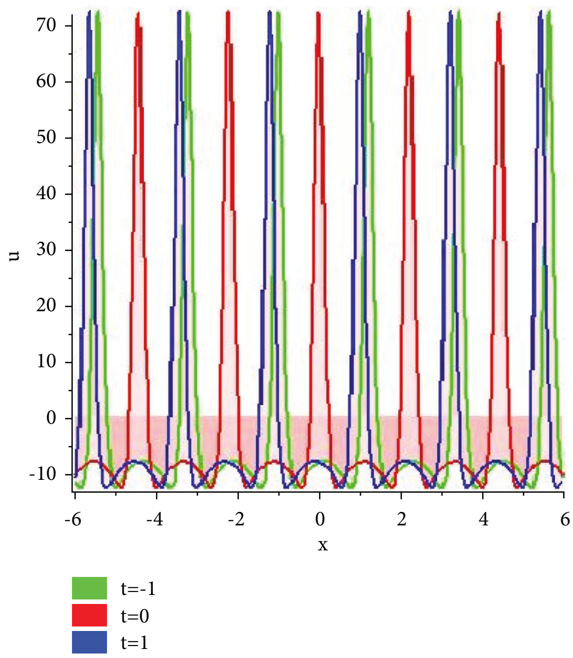

(e)

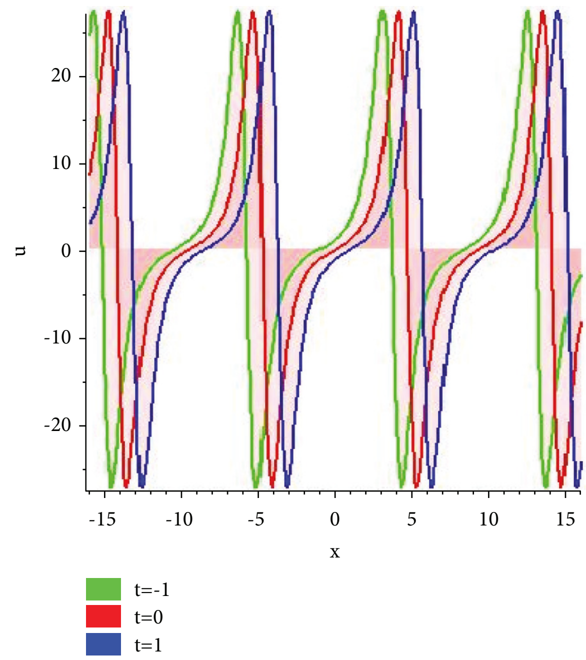

(f)

FIGURE 5: Periodic solution of equation (14) and the periodicity exist along the x-axis: (i) dark wave: 3D (upper) and contour (lower) plots, (iv) 2D plot of (i); (ii) bright wave: 3D (upper) and contour (lower) plots, (v) 2D plot of (ii); (iii) dark-Bright wave: 3D (upper) and contour (lower) plots, (vi) 2D plot of (iii).

(25), (26), and (27) arrived in the form of hyperbolic function under some conditions.

Solution (7) is a complex-valued function for $\beta < 0$ and $a_1^2\gamma^2 < 36\beta\alpha^2k^2$ or $\beta > 0$ and $a_1^2\gamma^2 > 36\beta\alpha^2k^2$ and it can be expressed as the trigonometric function in equations (7)–(9). The solutions (8) and (9) give periodic rogue waves solution as shown in Figure 4 for $c_1 = 1, c_2 = 2, k = \alpha = 0.5, a_1 = 3, \gamma = 1$ and $c_1 = 1, c_2 = 2, k = \alpha = 0.5, a_1 = 3, \gamma = 1$, respectively.

For $\beta < 0$ and $a_1^2\gamma^2 > 36\beta\alpha^2k^2$ or $\beta < 0$ and $a_1^2\gamma^2 < 36\beta\alpha^2k^2$, the solution (7) is a real-valued function solution, and it can be expressed as the hyperbolic function in equations (10)–(12). These solutions always provide different types of solitary waves.

Solution (14) is complex if $\alpha^2k^2 < \omega^2$ and it can be expressed as the trigonometric function in (15) and (16). The profile in Figures 5(a) and 5(d) is a 2D plot and 3D control plot of the real slice equation (14) for $c_1 = \gamma = 1, c_2 = 2, k = \alpha = \omega = 0.5, \beta = 3$ which is called a periodic solution. The 2D plot and 3D control plot of the real portion of equation (14) are a stable periodic solution for $c_1 = \gamma = 1, c_2 = 2, k = \alpha = \omega = 0.5$, and $\beta = 3$ in Figures 5(b) and 5(e). The profile in Figures 5(c) and 5(d) is the periodicity of the real portion of equation (14) for $\beta = 3. c_1 = \gamma = 1, c_2 = 2, k = \alpha = \omega = 0.5$, with 2D plot and 3D control plot.

For the condition $\alpha^2k^2 > \omega^2$, solution (14) can be expressed in the hyperbolic form in (18), (19), and (20). The solutions in (18) and (19) and the real part of (19) present bright and dark shape solution in Figures 6(a) and 6(c) and Figures 6(b) and 6(d) for $k = \alpha = 1, \gamma = 0.05, \beta = 1, \omega = 0.5$, taking the positive and negative signs of solutions, respectively.

The profile in Figure 7 represents density, three dimensional control plot, and 2D plot of the imaginary chunk of (20) for $c_1 = Ic_2 = 1, k = a_1 = \alpha = 1, \gamma = -1, \beta = -0.05$. Figure 4

For $\omega^2 < \beta$, the solution (22) is a complex valued function and it can be expressed as the trigonometric function in equations (22), (23), and (24). Solution (24) represents periodic rogue waves solution for $\omega = 0.5, \alpha = 2, \gamma = 1, \beta = 1$ and has a nature like Figure 4. The profile in Figure 8 is 3D contour plot and density plot of multitype lump wave solution of (25) for $\omega = 0.5, \alpha = 2, \gamma = 1, \beta = 1$. Figures 5–8.

4.2. Solutions via Dynamical System Scheme. In this subsection, we are going to visualize the nature of the solution that is achieved for each orbit with assorted values of the appreciate parameters. We see from the MSE scheme that a single solution changes into three different types of solutions due to a change in parametric conditions. But, this method initially bifurcated the phase orbits, and different types of orbits provided different types of solutions. The solutions (33), (35), (40), and (41) are consistent with homoclinic orbits and exhibit bell wave solutions, but (34) and (40) yield dark bell, while (36) and (41) yield bright bell wave envelops. The profile of dark bell solitary wave solution via (34) is shown in Figure 9. The profile of bright bell solitary wave solution via (36) is shown in Figure 10. Solutions (37) and

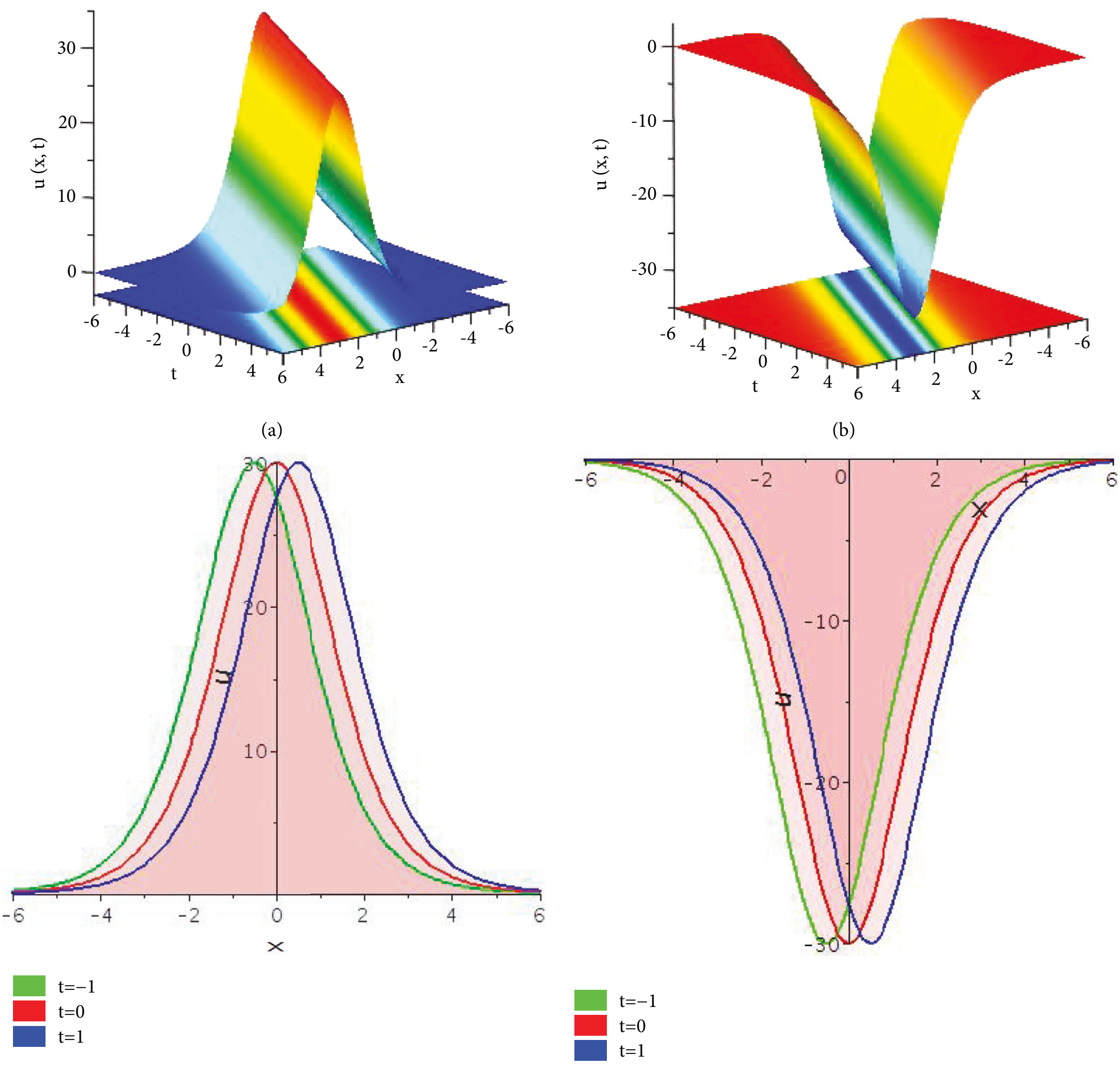

(a) (b) (c) (d)

FIGURE 6: Profile of solution of equation (18): (i) 3D (upper) and density (lower) plot as bright bell wave, (iii) 2D plot of (i); (ii) 3D (upper) and density (lower) plots as dark bell wave, (iii) 2D plots of (ii).

(38) exhibit a different type of periodic wave solutions which are depicted by Figures 11 and 12 respectively. Besides this, cusp orbit provided us cusp type peaked wave solutions (44) and (45) which are exploited in Figures 13 and 14, respectively. They exhibit upward and downward peaks as directions of orbits are opposite.

5. Remarks and Comparison

It is worth mentioning that both techniques we used here are very simple and direct and take less computational effort than the other methods [42, 44], and these techniques can be handled without help of the auxiliary equation to exhibit the internal mechanism of the model. Sirendaoreji [42] used the auxiliary method to solve the quadratic nonlinear KG model and extracted solitary, periodic, and singular solutions in real form only by getting the help of the auxiliary equation. Besides this, Zhang [44] solved the same model by using the exp-function method and extracted a few solutions, including solitary as well as periodic waves only in real form. But, our solutions obtained by the two methods found solitary, periodic, and singular solutions in both real and complex forms, which cover all of their solutions. In addition, we derived our results by direct integration from its Hamiltonian following each energy orbit of its phase portraits. We extracted different bounded and unbounded periodic waves, dark and bright bell shape, dark-bright and bright-dark kink wave, polynomial solution, disguise version of soliton, and periodic rouge wave resolutions of the KG model which was not reported in [42, 44].

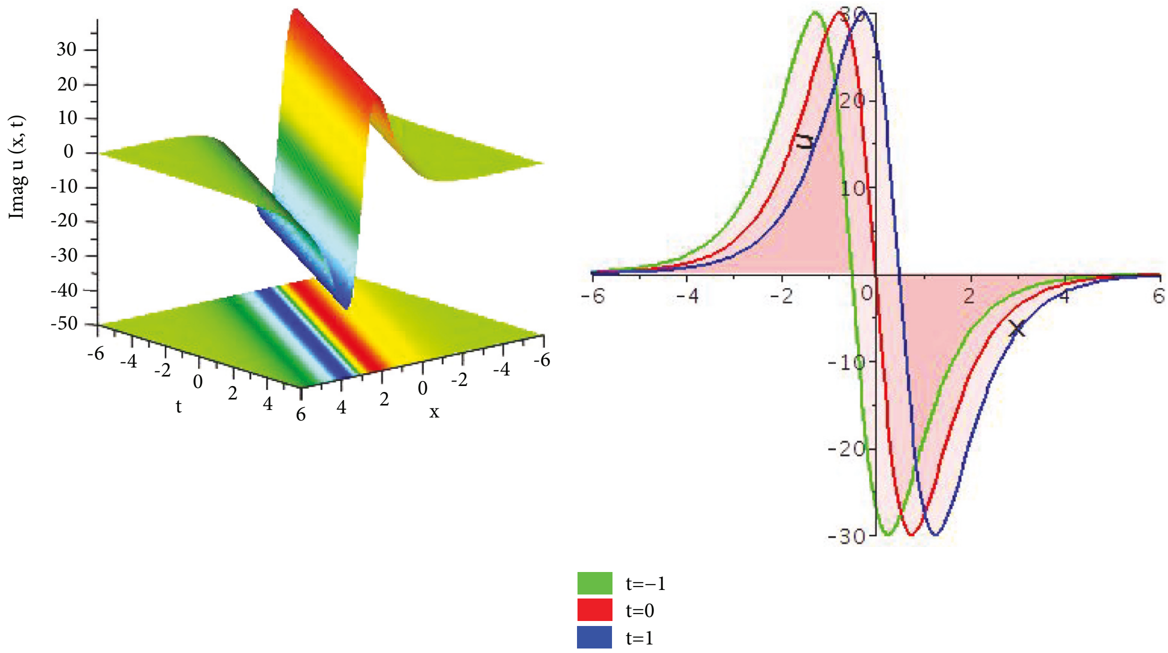

(a) (b)

Figure 7: The profile is the single soliton as a dark-bright kink wave of the imaginary portion of equation (19) for $c_1 = 1, k = \alpha = 1,\ \omega = 0.5, \gamma = 0.05, \beta = 1$: (i) 3D plot (upper) and contour plot (lower), (ii) 2D plot.

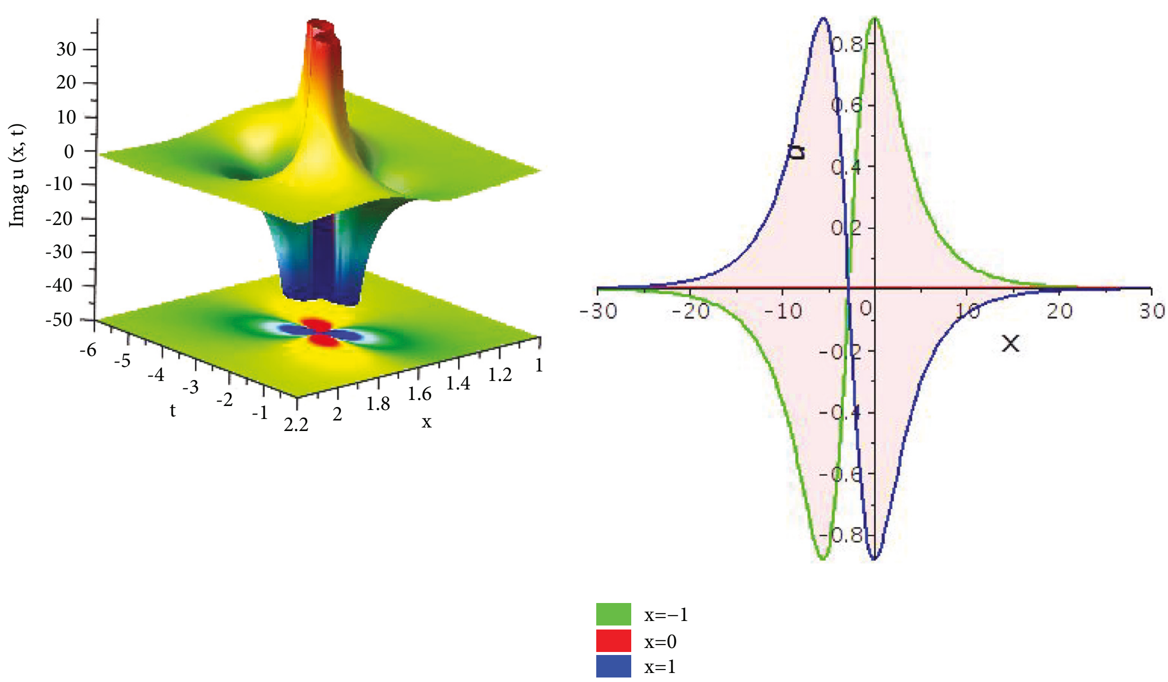

(a) (b)

Figure 8: Multilump wave solution of solution (24) for $\gamma = 1, \beta = 1.\ k = \alpha = 0.5$. The periodicity exists along the x-axis: (i) 3D plot (upper) and density plot (lower), (ii) 2D plot.

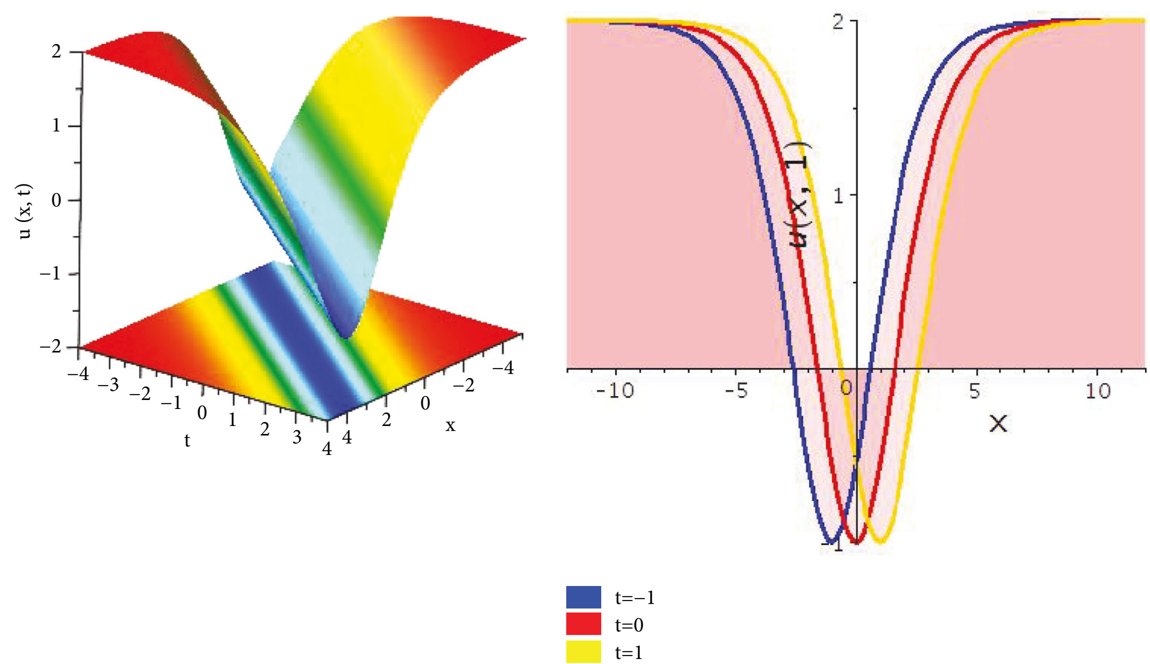

(a) (b)

Figure 9: Shapes of the solution of equation (33): (a) 3D shape (upper), density (lower) plots of dark bell wave, and (b) 2D shape for $\alpha = 2, \beta = -2, \gamma = -1, \omega = k = 1$.

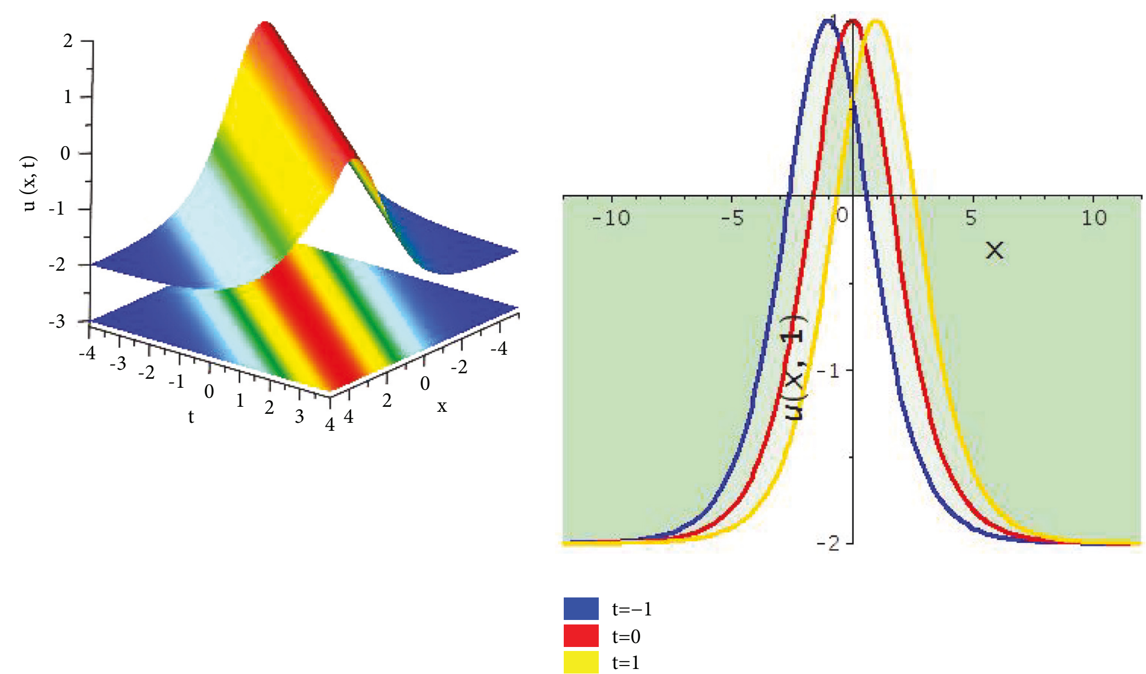

(a) (b)

Figure 10: Shapes of the solution of equation (35): (a) 3D shape (upper), density (lower) plots of bright bell wave, and (b) 2D shape for $\alpha = 2, \beta = -2, \gamma = \omega = k = 1$.

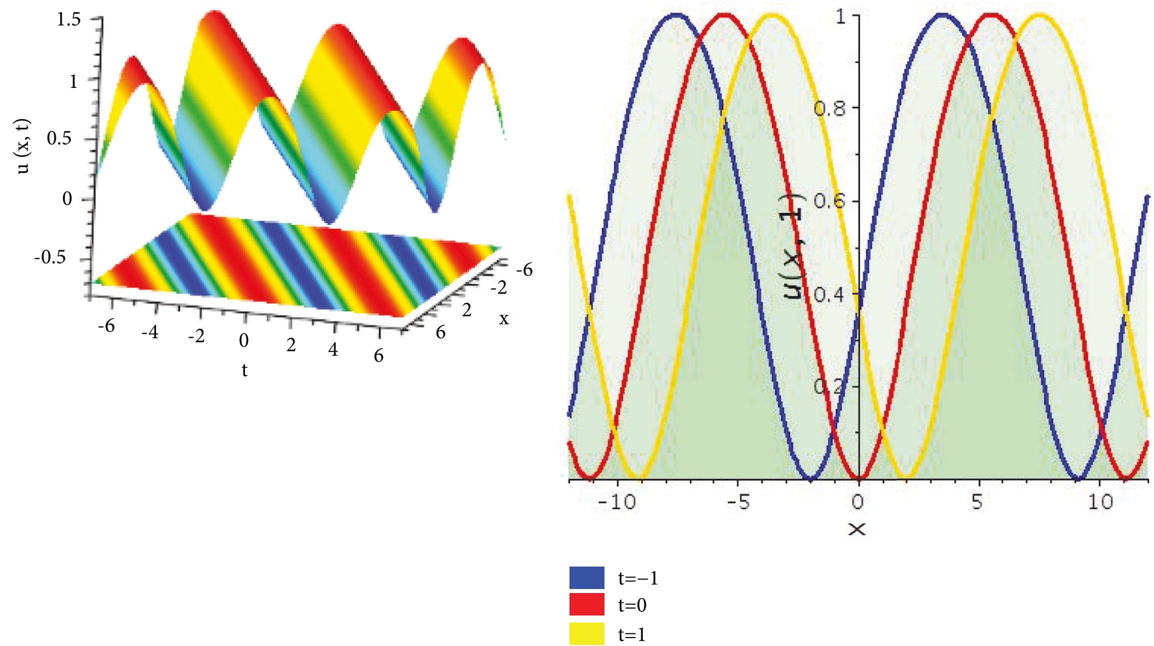

(a)

(b)

FIGURE 11: Shapes of the solution of equation (38): (a) 3D shape (upper), density (lower) plots of periodic wave, and (b) 2D shape for $\alpha = \beta = \gamma = k = 1, \omega = 2, l_1 = 0, l_2 = 1, l_3 = 2$.

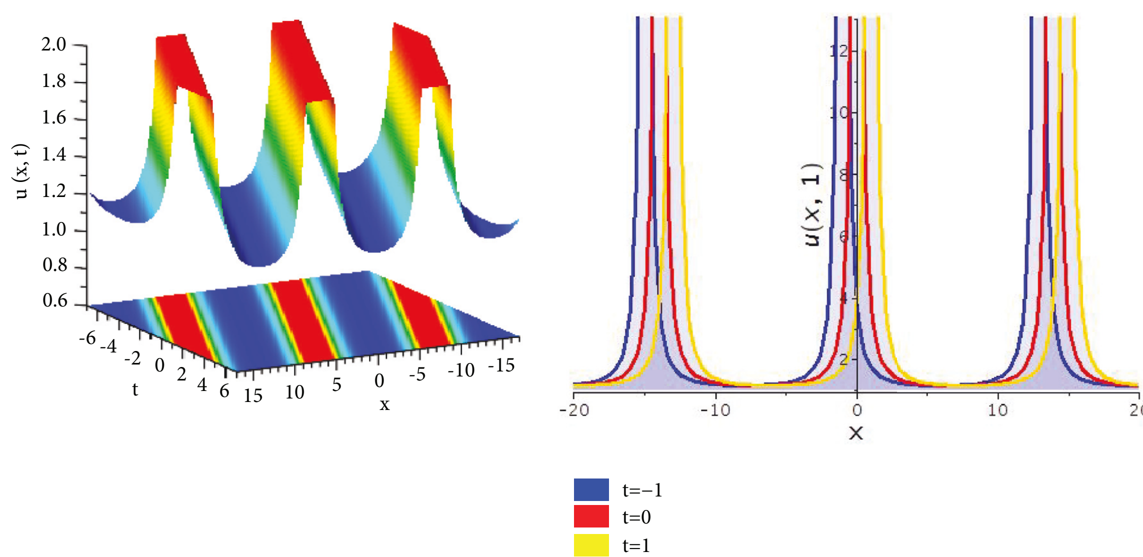

(a)

(b)

FIGURE 12: Shapes of the solution of equation (37): (a) 3D shape (upper), density (lower) plots of periodic wave, and (b) 2D shape for $\alpha = 2, \beta = \gamma = k = \omega = 1, l_4 = 0.8, l_5 = 1.1, l_6 = 3$.

6. Conclusion

In this research, we successfully investigated the quadratic nonlinear KG model with bifurcation analysis. The MSE and dynamical system schemes are employed in the model and extracted different bounded and unbounded periodic waves, dark and bright bell shape, dark-bright and bright-dark kink wave, disguise version of soliton, and periodic rouge wave resolutions of the KG model. We apply the dynamical system to bifurcate the model and draw distinct phase portraits on unlike parametric constraints. Following each orbit of all phase portraits, we originate

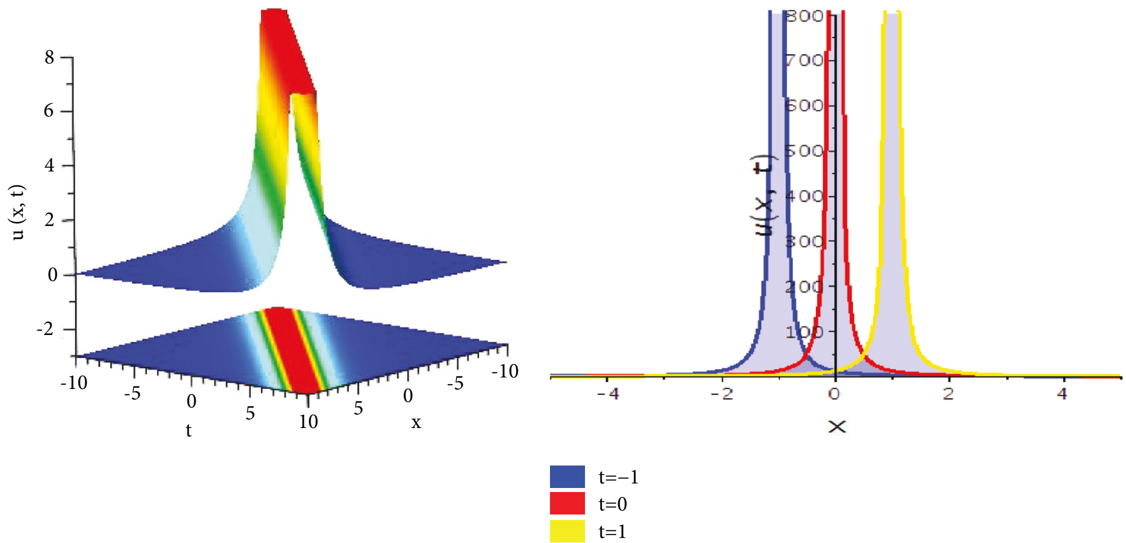

(a) (b)

FIGURE 13: Shapes of the solution of equation (44): (a) 3D shape (upper), density (lower) plots of periodic wave, and (b) 2D shape for $\alpha = 3, \beta = 2, \gamma = -4, k = \omega = 1$.

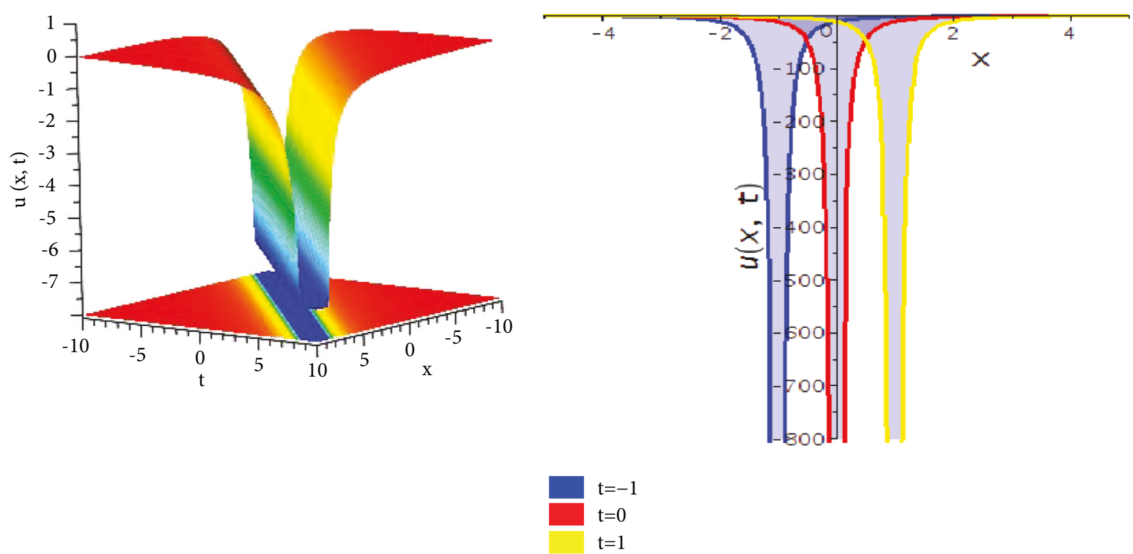

(a) (b)

FIGURE 14: Shapes of the solution of equation (45): (a) 3D shape (upper), density (lower) plots of periodic wave, and (b) 2D shape for $\alpha = 3, \beta = 2, \gamma = 4, k = \omega = 1$.

bounded and unbounded solitary, periodic and periodic rogue-type wave solutions of the KG model. We also analyze the effect of parameters on the obtained wave solutions and discuss why and when it changes its self-nature. Numerical illustrations of the derived solutions with 3D contour, density, and 2D plots are presented by the arbitrary picking of parameters allied with conditions. Lastly, we think that the realized schemes are burly and more skilled than other schemes and the attained solutions are reliable.

Data Availability

Supported data are available in the links (as it is Maple code, one can open it in Maple software only): https://www.dropbox.com/s/gcox6xtfzw0pq4k/Fig% 201%203d%20DSM.mw?dl = 0 and https://www.dropbox.com/s/w7rh66pj4hqz3xh/Fig% 201%20bifer.mw?dl = 0.

Conflicts of Interest

The authors declare no conflicts of interests.

Authors' Contributions

M.M. Hossain developed the methodology and validated the study; A. Abdeljabbar conceptualized the study, developed software, and did funding acquisition; M. Roshid supervised the study, wrote the original draft, and did checking; H.O. Roshid is the idea maker, validated the study, and curated the data; A.N. Sheikh supervised and finalized the study. All authors have read and agreed to the published version of the manuscript.

Acknowledgments

The authors are grateful to Khalifa University, Abu Dhabi, United Arab Emirates, for their financial support that helped them in the quality research and presentation of this paper. This research was partially funded by the Deanship of Khalifa University, Abu Dhabi, the United Arab Emirates.

References

[1] M. Rudolph-Lilith, "A discrete algebraic framework for stochastic systems which yield unique and exact solutions," *Heliyon*, vol. 4, no. 7, Article ID e00691, 2018.
[2] J. Dvornik, A. Jaguljnjak Lazarevic, D. Lazarevic, and M. Uros, "Exact arithmetic as a tool for convergence assessment of the IRM-CG method," *Heliyon*, vol. 6, no. 1, Article ID e03225, 2020.
[3] W. X. Ma and J. H. Lee, "A transformed rational function method and exact solutions to the 3+1 dimensional Jimbo–Miwa equation," *Chaos, Solitons & Fractals*, vol. 42, no. 3, pp. 1356–1363, 2009.
[4] Y. J. Yang, "The fractional residual method for solving the local fractional differential equations," *Thermal Science*, vol. 24, no. 4, pp. 2535–2542, 2020.
[5] S. O. Akindeinde, "A new multistage technique for approximate analytical solution of nonlinear differential equations," *Heliyon*, vol. 6, no. 10, Article ID e05188, 2020.
[6] L. Ali, S. Islam, T. Gul, M. A. Khan, and E. Bonyah, "Solutions of nonlinear real-world problems by a new analytical technique," *Heliyon*, vol. 4, no. 11, Article ID e00913, 2018.
[7] A. M. Wazwaz, "The extended tanh method for abundant solitary wave solutions of nonlinear wave equations," *Applied Mathematics and Computation*, vol. 187, no. 2, pp. 1131–1142, 2007.
[8] H. O. Roshid, M. H. Khan, and A. M. Wazwaz, "Lump, multi-lump, cross kinky-lump and manifold periodic-soliton solutions for the (2+1)-D Calogero–Bogoyavlenskii–Schiff equation," *Heliyon*, vol. 6, no. 4, Article ID e03701, 2020.
[9] M. S. Ullah, M. Zulfikar Ali, H. O. Roshid, A. R. Seadawy, and D. Baleanu, "Collision phenomena among lump, periodic and soliton solutions to a (2 + 1)-dimensional Bogoyavlenskii's breaking soliton model," *Physics Letters A*, vol. 397, Article ID 127263, 2021.
[10] M. S. Ullah, M. Z. Ali, H. O. Roshid, and M. F. Hoque, "Collision phenomena among lump, periodic and stripe soliton solutions to a (2 + 1)-dimensional Benjamin–Bona–Mahony–Burgers Model," *The European Physical Journal Plus*, vol. 136, no. 4, p. 370, 2021.
[11] Y. Yıldırım, E. Yaşar, and Y. Zhang, "Multiple exp-function method for soliton solutions of nonlinear evolution equations," *Chinese Physics B*, vol. 26, no. 7, Article ID 070201, 2017.
[12] M. T. Darvishi, M. Najafi, and M. Najafi, "Application of multiple Exp-Function method to obtain multi-soliton solutions of (2 + 1)- and (3 + 1)-Dimensional Breaking Soliton equations," *American Journal of Computational and Applied Mathematics*, vol. 1, no. 2, pp. 41–47, 2012.
[13] M. Gaballah, R. M. El-Shiekh, L. Akinyemi, and H. Rezazadeh, "Novel periodic and optical soliton solutions for Davey–Stewartson system by generalized Jacobi elliptic expansion method," *International Journal of Nonlinear Sciences and Numerical Stimulation*, 2022.
[14] M. Arshad, A. R. Seadawy, D. Lu, and M. S. Saleem, "Elliptic function solutions, modulation instability and optical solitons analysis of the paraxial wave dynamical model with kerr media," *Optical and Quantum Electronics*, vol. 53, no. 1, p. 7, 2021.
[15] S. Kumer and M. Niwas, "Exact closed-form solutions and dynamics of solitons for a (2+1)-dimensional universal hierarchy equation via Lie approach," *Pramana - Journal of Physics*, vol. 95, p. 195, 2021.
[16] S. Kumer and S. S. Dhiman, "Lie symmetry analysis, optimal system, exact solutions and dynamics of solitons of a (3 + 1)-dimensional generalised BKP–Boussinesq equation," *Pramana - Journal of Physics*, vol. 96, p. 31, 2022.
[17] S. Kumar and A. Kumar, "Abundant closed-form wave solutions and dynamical structures of soliton solutions to the (3+1)-dimensional BLMP equation in mathematical physics," *Journal of Ocean Engineering and Science*, vol. 7, no. 2, pp. 178–187, 2022.
[18] L. Ouahid, M. A. Abdou, S. Owyed, and S. Kumar, "New optical soliton solutions via two distinctive schemes for the DNA Peyrard–Bishop equation in fractal order," *Modern Physics Letters B*, vol. 35, no. 26, Article ID 2150444, 2021.
[19] S. Kumar, "Some new families of exact solitary wave solutions of the Klein–Gordon–Zakharov equations in plasma physics," *Pramana - Journal of Physics*, vol. 95, no. 4, p. 161, 2021.
[20] M. M. Roshid and H. O. Roshid, "Exact and explicit traveling wave solutions to two nonlinear evolution equations which describe incompressible viscoelastic Kelvin-Voigt fluid," *Heliyon*, vol. 4, no. 8, Article ID e00756, 2018.
[21] H. O. Roshid, M. M. Roshid, N. Rahman, and M. R. Pervin, "New solitary wave in shallow water, plasma and ion acoustic plasma via the GZK-BBM equation and the RLW equation," *Propulsion and Power Research*, vol. 6, no. 1, pp. 49–57, 2017.
[22] A. Ali, N. Ali, and A. M. Wazwaz, "Closed form traveling wave solutions of non-linear fractional evolution equations through the modified simple equation method," *Thermal Science*, vol. 22, no. Suppl. 1, pp. 341–352, 2018.
[23] R. M. El-Shiekh, M. Gaballah, and A. F. Elelamy, "Similarity reductions and wave solutions for the 3D-Kudryashov–Sinelshchikov equation with variable-coefficients in gas

bubbles for a liquid," *Results in Physics*, vol. 40, Article ID 105782, 2022.

[24] R. M. El-Shiekh and M. Gaballah, "New analytical solitary and periodic wave solutions for generalized variable-coefficients modified KdV equation with external force term presenting atmospheric blocking in oceans," *Journal of Ocean Engineering and Science*, vol. 7, no. 4, pp. 372–376, 2022.

[25] R. M. El-Shiekh, "Novel solitary and shock wave solutions for the generalized variable-coefficients (2+1)-dimensional KP-Burger equation arising in dusty plasma," *Chinese Journal of Physics*, vol. 71, pp. 341–350, 2021.

[26] M. B. Hossen, H. O. Roshid, and M. Z. Ali, "Characteristics of the solitary waves and rogue waves with interaction phenomena in a (2 + 1)-dimensional Breaking Soliton equation," *Physics Letters A*, vol. 382, no. 19, pp. 1268–1274, 2018.

[27] S. Ali, M. O. Younis, M. O. Ahmad, and S. T. R. Rizvi, "Rogue wave solutions in nonlinear optics with coupled Schrödinger equations," *Optical and Quantum Electronics*, vol. 50, no. 7, p. 266, 2018.

[28] Y. Ohta and B. F. Feng, "General rogue wave solutions to the discrete nonlinear Schrödinger equation," 2022, https://arxiv.org/abs/2201.02359.

[29] R. F. Zhang, M. C. Li, and H. M. Yin, "Rogue wave solutions and the bright and dark solitons of the (3+1)-dimensional Jimbo–Miwa equation," *Nonlinear Dynamics*, vol. 103, no. 1, pp. 1071–1079, 2021.

[30] Q. Lu, O. A. Ilhan, J. Manafian, and L. Avazpour, "Multiple rogue wave solutions for a variable-coefficient Kadomtsev–Petviashvili equation," *International Journal of Computer Mathematics*, vol. 98, no. 7, pp. 1457–1473, 2021.

[31] A. Degasperis, S. Lombardo, and M. Sommacal, "Rogue wave type solutions and spectra of coupled nonlinear Schrödinger equations," *Fluid*, vol. 4, no. 1, pp. 57–77, 2019.

[32] A. Ankiewicz and N. Akhmediev, "Rogue wave solutions for the infinite integrable nonlinear Schrödinger equation hierarchy," *Physical Review E - Statistical Physics, Plasmas, Fluids, and Related Interdisciplinary Topics*, vol. 96, no. 1, Article ID 012219, 2017.

[33] A. Yusuf, T. Sulaiman, A. Abdeljabbar, and M. Alquran, "Breather waves, analytical solutions and conservation laws using Lie–Bäcklund symmetries to the (2 + 1)-dimensional Chaffee–Infante equation," *J. Ocean Engineer. Sci.*, 2022, in press.

[34] T. A. Sulaiman, A. Yusuf, A. Abdeljabbar, and M. Alquran, "Dynamics of lump collision phenomena to the (3+1)-dimensional nonlinear evolution equation," *Journal of Geometry and Physics*, vol. 169, Article ID 104347, 2021.

[35] A. Abdeljabbar, "New double Wronskian exact solutions for a generalized (2+1)-dimensional nonlinear system with variable coefficients," *Partial Differential Equations in Applied Mathematics*, vol. 3, Article ID 100022, 2021.

[36] A. Abdeljabbar and T. D. Tran, "Pfaffian solutions to a generalized KP system with variable coefficients," *Applied Mathematical Sciences*, vol. 10, no. 48, pp. 2351–2368, 2016.

[37] R. M. El-Shiekh and M. Gaballah, "New rogon waves for the non-autonomous variable coefficients Schrödinger equation," *Optical and Quantum Electronics*, vol. 53, no. 8, p. 431, 2021.

[38] I. Ahmed, A. R. Seadawy, and D. Lu, "M-shaped rational solitons and their interaction with kink waves in the Fokas–Lenells equation," *Physica Scripta*, vol. 94, no. 5, Article ID 055205, 2019.

[39] W. G. Zhang, X. Q. Ling, X. Li, and S. W. Li, "The orbital stability of solitary wave solutions for the generalized Gardner equation and the influence caused by the interactions between nonlinear terms," *Complexity*, vol. 2019, Article ID 4209275, 17 pages, 2019.

[40] M. Kirane and A. Abdeljabbar, "Nonexistence of global solutions of systems of time fractional differential equations posed on the Heisenberg group," *Mathematical Methods in the Applied Sciences*, 2022, in press.

[41] K. C. Basak, P. C. Ray, and R. K. Bera, "Solution of non-linear klein–gordon equation with a quadratic non-linear term by Adomian decomposition method," *Communications in Nonlinear Science and Numerical Simulation*, vol. 14, no. 3, pp. 718–723, 2009.

[42] Sirendaoreji, "Auxiliary equation method and new solutions of klein–gordon equations," *Chaos, Solitons & Fractals*, vol. 31, no. 4, pp. 943–950, 2007.

[43] N. Hayashi and P. I. N. Aumkin, "Quadratic nonlinear klein-gordon equation in 2d Cauchy problem," *Adv. Stud. Pure Math.*vol. 64, pp. 89–100, 2015.

[44] S. Zhang, "Exp-function method for Klein–Gordon equation with quadratic nonlinearity," *Journal of Physics: Conference Series*, vol. 96, Article ID 012002, 2008.

[45] H. Bin, L. Jibin, L. Yao, and R. Weiguo, "Bifurcations of travelling wave solutions for a variant of Camassa-Holm equation," *Nonlinear Analysis: Real World Applications*, vol. 9, no. 2, pp. 222–232, 2008.